PAPER

Fabrication of superhydrophobic surface by oxidation growth of flower-like nanostructure on a steel foil

Rui Weng, [a] Haifeng Zhang, [*a] Liang Yin,[a] Wanting Rong,[a] Zhiwen Wu[a] and Xiaowei Liu[ab]

Energy saving has drawn attention all around the world. The fluidic drag reduction effect of superhydrophobic surfaces has been investigated both theoretically and experimentally. However, there has been little experimental analysis on the drag reduction of superhydrophobic steel surfaces. Here, we present a novel method to fabricate the superhydrophobic surface with a 3D flower-like micro-nanostructure on the steel foil using the method of high-temperature oxidation. The wettability of the oxide films can be easily changed from super hydrophilic to superhydrophobic with chemical modification. We measure the liquid/solid friction of the as-prepared superhydrophobic surface using the self-assembly system. The drag reduction ratio for the superhydrophobic steel surface is 20–30% at low velocity. The superhydrophobic steel surface has numerous technical applications in drag reduction field.

1. Introduction

Water and its interaction with solid surfaces induce frictional resistance. Frictional drag accounts for 60–70% of the total drag on a cargo ship, about 80% for a tanker and 90% for underwater vehicles.[1,2] In marine vessels, more than half of the energy used for propulsion is wasted on overcoming surface friction. Drag reduction in fluid flow is a fundamental issue in the field of process engineering, and achieving drag reduction will benefit a multitude of industries.[3–6] In recent years, drag reduction research has received considerable attention, in large part because it can help to reduce the large fuel consumption. As a fundamental property of a solid surface, wettability plays an important role in liquid/solid friction drag. Over the past decades, many researchers such as Barthlott and Jiang have performed extensive research on the wettability.[7–14] The superhydrophobic surface provides lubrication by the stable air layer on its surface. Water droplets can be rolled faster than other surfaces. Experiments indicated that superhydrophobic surfaces had considerable friction drag reduction effect. The drag reduction ability of superhydrophobic surfaces has garnered more attention, and it has been widely investigated in the past decade.

The steel is widely used in many engineering fields, the fabrication of superhydrophobic steel surfaces has attracted much attention because of their practical applications in fluid

drag reduction, anticorrosion, no-loss transportation and so forth.[15,16] Liu proposed a simple method to fabricate superhydrophobic surfaces on SS 304 with micro–nano structure by chemical etching.[17] Jagdheesh studied the effect of laser-patterned nanoscale structures on the wetting behavior of silanized stainless steel.[18] Liang presented a method to prepare the stable superhydrophobic surface on the SS 316L substrate by a combined approach using electrodeposition and fluorinated modification.[19] However, the severe preparation conditions, multistep processes, expensive low surface energy materials, harsh chemical treatment and the high cost of the previous methods limit the practical application of superhydrophobic surfaces over large areas.[20] Most research on the drag-reducing effect of superhydrophobic surfaces was carried out by investigating flow behaviors on static superhydrophobic surfaces and demonstrated the dynamic drag-reducing property of superhydrophobic coatings under this condition except Steinberger's report. However, there has been little the investigation of movement behaviors on the superhydrophobic surfaces. We develop a simple method fabricating superhydrophobic surface with 3D flower-like micro–nanostructure on a steel foil in this paper. We hope that our findings can provide a better understanding of superhydrophobic properties and be useful in further research on drag-reducing materials.

2. Experimental

2.1 Materials and methods

The thermal oxidation process was used to synthesize the micro/nanoscale hierarchical structures. The schematic diagram of the experimental setup is shown in Fig. 1. The experimental setup

[a]*MEMS Center, Harbin Institute of Technology, Harbin, 150001, China. E-mail: zhanghf@hit.edu.cn*

[b]*State Key Laboratory of Urban Water Resource & Environment, (Harbin Institute of Technology), Harbin, 150001, China*
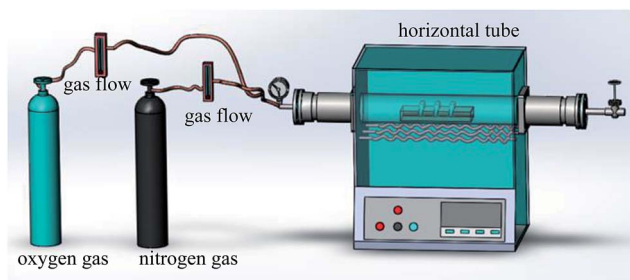
Fig. 1 Schematic representation of the experimental setup.

included a horizontal tube furnace, a quartz tube 100 cm in length and 12 cm in diameter, and a gas flow/control system. 50# carbon steel foils were used as the substrates.[21] The steel foils with a size of 25 mm × 30 mm × 0.3 mm were polished with 400#, 800#, and 1500# sandpaper in turn. The steel foils were cleaned with absolute ethanol in an ultrasound bath before being loaded into a quartz boat. The oxidized sample was positioned at the end of the quartz tube. The quartz tube was then mounted in the middle of the tube furnace. The temperature (500 °C), pressure (1 atm), and reacting time were controlled. High-purity nitrogen was first introduced into the quartz tube to remove the air in the system. The samples were then heated comprising a flow gas mixture 24 sccm N_2 gas and 6 sccm O_2 gas. After being held at this temperature for different reaction time the N_2 gas was kept flowing, and the O_2 flow was stopped. The samples were cooled to room temperature. The oxidized steel foils were carefully cleaned with ethanol in an ultrasound bath. Finally, as-prepared samples were modified using an ethanol solution of fluorinated silane (FAS, 1H,1H,2H,2H-per-fluorooctadecyltrichlorosilane) of 0.6 wt% for 30 min. The samples were dried in the vacuum oven at 120 °C for 60 min. The superhydrophobic steel surface was thus obtained.

2.2 Sample characterization

The scanning electron microscope (SEM, Tescan VEGA 3 SBH) equipped with energy dispersive X-ray spectroscopy (EDX, Thermo Scientific) was employed to examine the surface morphology and the chemical constitution of as-prepared samples. The X-ray diffraction (XRD) patterns of the samples were recorded with a Bruker D8 Advance diffractometer. The CAs of water droplets were measured by an optical contact angle meter system (Data Physics Instrument GmbH, Germany) at ambient temperature using the Laplace–Young fitting model for the static CAs. The water CA and SA reported here were the mean values measured with 5 μL of water droplets at five different positions on each test surface. To investigate the drag reduction of the superhydrophobic film, the self-assembly system was used to measure the drag of as-prepared film.

3. Results and discussion

Fig. 2 shows SEM images of the samples prepared with different oxidation time at 500 °C (24 sccm of N_2 and 6 sccm of O_2), (a) 0 h (b) 5 h (c) 10 h. Fig. 2(a) is the micrograph of the steel surface
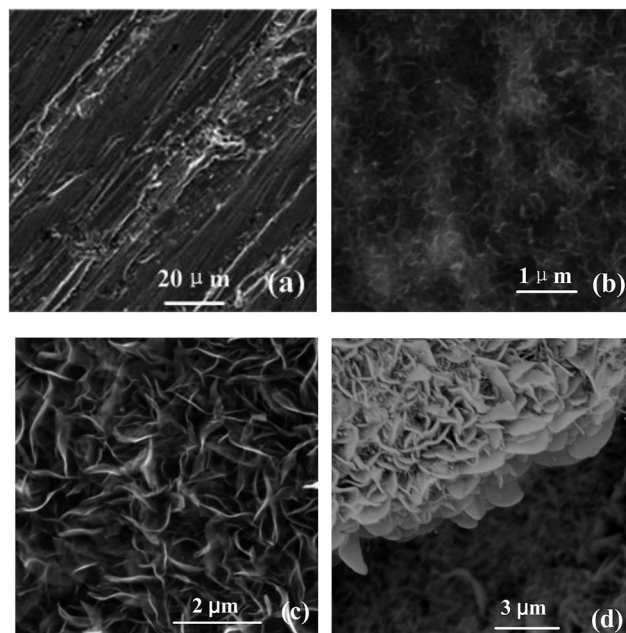

Fig. 2 (a) SEM images for polished samples (b) SEM images for the prepared samples with oxidation time for 5 h at 500 °C (24 sccm of N_2 and 6 sccm of O_2) (c) SEM images for the prepared samples with oxidation time for 10 h at 500 °C (24 sccm of N_2 and 6 sccm of O_2) (d) cross-section view of oxidation sample for 10 h at 500 °C.

after sandpaper treatment and cleaning. It shows that the steel surface is relatively smooth, only some scars by sandpaper polishing process. When the reaction time is short (5 h), the nanosheets is sparsely covered with some flower-like nanostructures. When the reaction time is prolonged to 10 h, more and more nanoflowers are formed, and their size grows bigger gradually (Fig. 2(c)). The nanowall cross-section view (Fig. 2(d)) of the sample oxidation time 10 h at 500 °C shows that the height of the nanowalls is around 2 μm. Rough structures are obvious in the cross section view shown in Fig. 2(d). This type of hierarchical nanostructure provides sufficient roughness to stably entrap the air to enhance the hydrophobic of the surface.

This Fig. 3(a) shows the EDX spectrum of the oxidized steel surface, which reveals the presence of O and Fe elements. Quantitative results show that the value of the atomic ratio of Fe : O is ∼1.496. The sample was subjected to XRD measurements to confirm the chemical composition of the nanosheets. Fig. 3(b) shows typical XRD peaks of both Fe substrate (gray line) and as-synthesized sample. Magnetite is believed to be the primary crystalline phase for the synthesized nanosheets as identified by the new diffraction peaks at 33.1°, 35.6°, 43.5°, 49.4°, 64.0° and 82.97°. These peaks correspond to five indexed planes (104), (110), (202), (024), and (300), (210) respectively. They can be perfectly indexed to a rhombohedral Fe_2O_3 structure with lattice parameters $a = 0.5038$ nm and $c = 1.3772$ nm. It can be seen that both EDX spectrum and XRD patterns are in conformity with Fe_2O_3.

The chemical compositions of the resulting superhyphobic surfaces are analyzed by XPS. Fig. 4 shows the XPS survey spectrum of the chemical composition on the synthesized
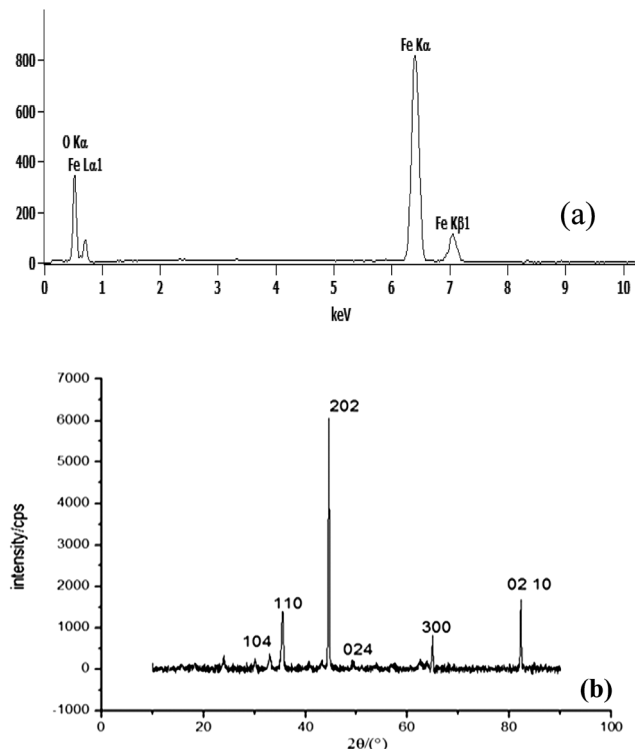
Fig. 3 (a) EDX spectrum and (b) XRD patterns of the steel foil prepared *via* oxidation process.

Fig. 5 The photographs of the 5 μL water droplet on (a) the bared steel foil, (b) the resultant oxide film and (c) the oxide film after FAS modification. (d) A photograph of water droplets on the superhydropobic steel surface.

Fig. 6 Mechanical stability of the as-prepared surface. (a) SEM image of sample before oscillating ultrasonic. (b) SEM image of sample oscillating in ultrasonic 5 min.

surfaces. There are three peaks: C1s, O1s, Fe2p (Fig. 4(a)). Fig. 4(b) shows the XPS spectrum of the Fe2p region for the as-prepared surface. It shows Fe2p of peak values at binding energies of 724.28 and 710.68 eV, which are characteristic for Fe^{3+} in Fe_2O_3. The binding energies and linetype of Fe2p kernel standard are consistent with the document values for α-Fe_2O_3.[22] XPS analysis (Fig. 4(b)) demonstrated that the resulting super-hydrophobic surface, from which the nanoflower structures are grown, is also α-Fe_2O_3 with comparatively small crystal size and plentiful intergranular–intercrystalline porosity. The resulting surface can possibly supply conveyance of Fe and O for α-Fe_2O_3 synthesized nanosheets growth.
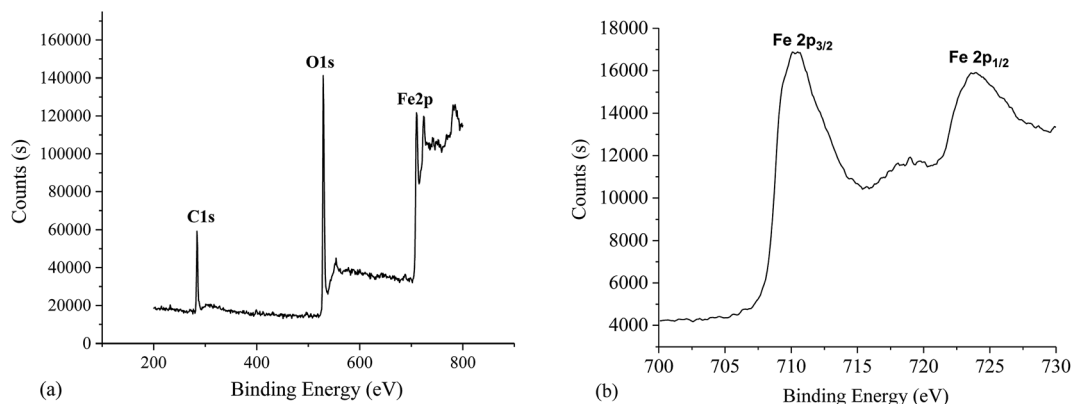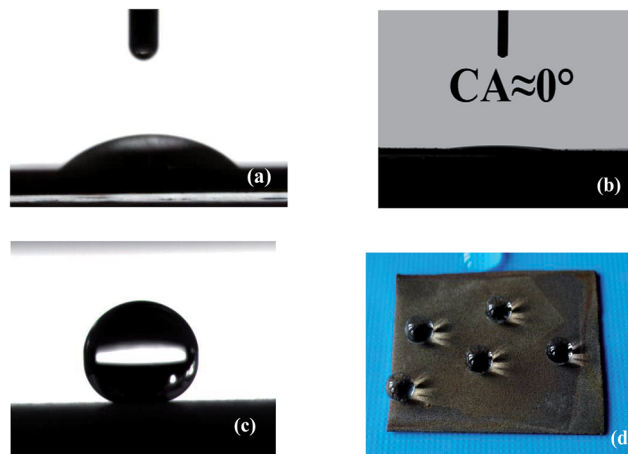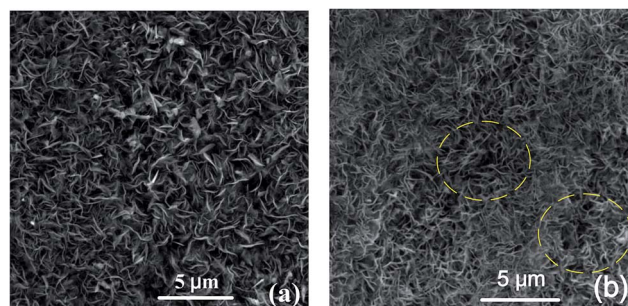
The wettability of steel surfaces was evaluated by the water static contact angle. The untreated steel has a water contact angle of about 20°. After the high-temperature oxidation, the surface of the steel shows water CAs of approximate 0°. The wettability of the steel foil is successfully converted from

Fig. 4 XPS spectrum of the synthesized nanosheets surface of a (a) full-spectrum and (b) Fe2p.

superhydrophilicity to superhydrophobicity by modified the silane reagent. The average CA increases from 0° to 158 ± 2°. Fig. 5(d) showed optical image 10 μL water droplets on the superhydrophobic surface. From the Fig. 5(d), many water droplets present round shapes with large CAs.
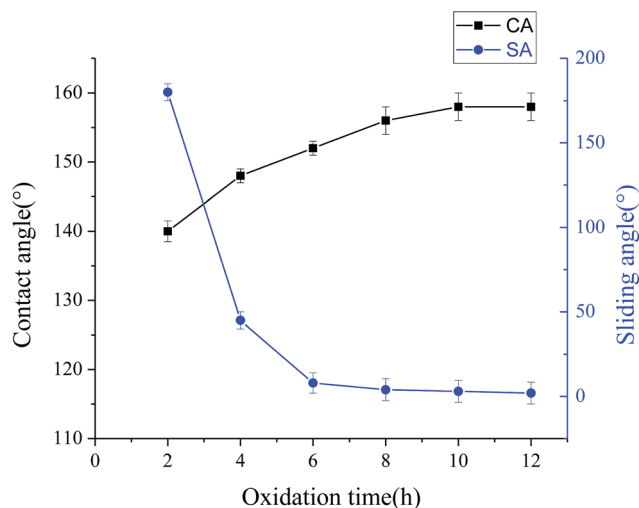
Mechanical stability is an important characteristic of the resulting superhydrophobic surfaces. Ultrasonic oscillation had been used to explore the mechanical stability of the as-prepared surfaces. We used the sample which was oxidized for 10 hours and put the same samples into ethanol and ultrasonic oscillate (KQ-50B) for 5 min. Fig. 6(b) shows the SEM images of the sample after the ultrasonic oscillation. There are few nanowalls to be damaged, which can be observed particularly in two circular areas highlighted in Fig. 6(b). We can see that the sample still keep the original shape. Accordingly, the high mechanical stability of the resulting surfaces had been confirmed by ultrasonic oscillation experiments.

The reaction time has a distinct influence on the surface wettability. Fig. 7 shows the change of the water CA and SA on the modified steel surface with the different oxidation time at 500 °C. It can be found from Fig. 7 that the water contact angle has reached 150 ± 2° for the sample that only treated for 6 h. As the test time increased, the as-prepared steel foil exhibited a decline trend in the SAs. The water sliding angle reduces to approximately 2° as the minimum value for 12 h. The hydrophobicity of a surface will be enhanced by increasing the surface roughness. The trapped air in the micro–nano structure can minimize the contact area between the solid surface and the water droplet. The water CA of the resultant surface increases with increasing reaction time.
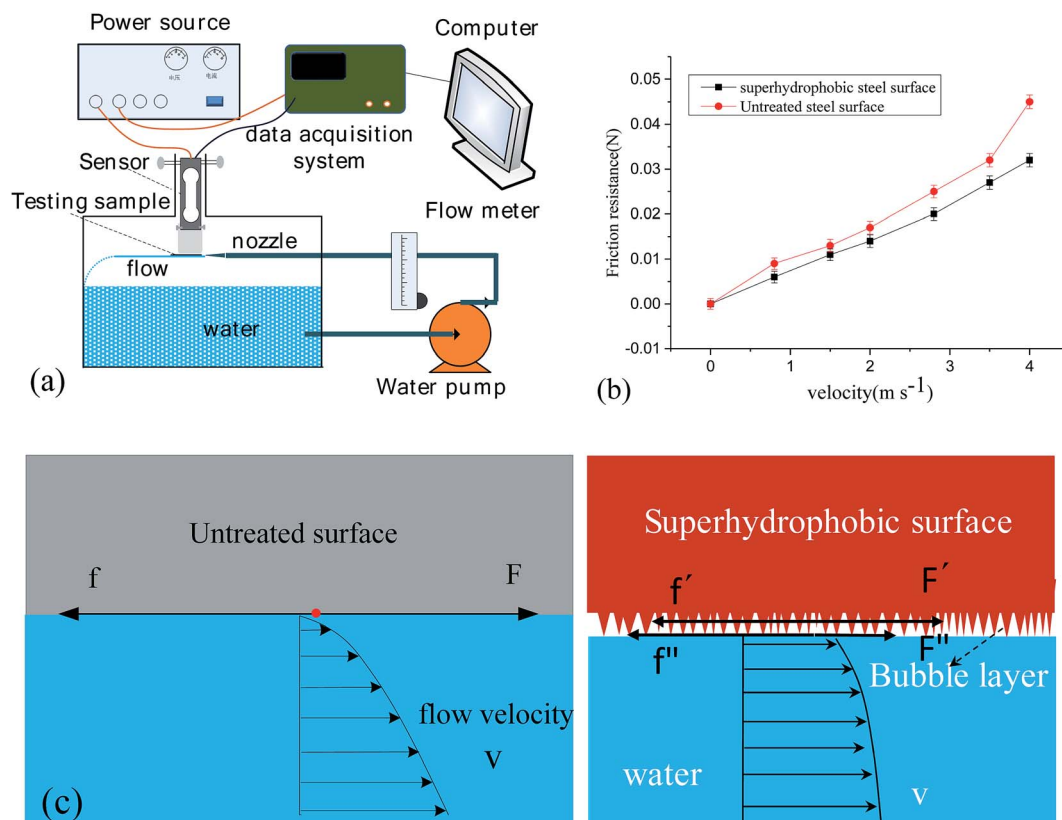

Fig. 7 Relationship between the water CA and SA of the as-prepared steel foil and the reaction time at 500 °C. Samples have been modified by fluorinated silane after chemical etching and oxidation.

Fig. 8 (a) Schematic of the frictional measurement. (b) Friction drag *versus* the velocity of the water flowing over surfaces with different adhesion property. (c) Drag reducing mechanism of the superhydrophobic surface.

The non-sticking property of the superhydrophobic surface is analyzed using the method proposed by McCarthy.[23] According to the approach, contact and departure processes of a 5 μL water droplet on the modified Fe_2O_3 nanosheet surfaces. The suspended water droplet is first contacted with the elevating superhydrophobic substrate. We find that the water droplet suspended the needle is hard to be pulled down to the Fe_2O_3 nanosheets surface. The as-prepared surface has no adhesive force to the water droplet, and exhibits excellent water repellency characteristics.

To investigate the liquid/solid friction of the superhydrophobic surface, the experimental setup of measuring the friction is reported in previous paper (Fig. 8(a)).[24] The friction resistance of solid–liquid interface was measured for 5 s under constant flow rate. The average values were calculated as the friction resistance of the as-prepared surface. Moreover, the interface friction was measured with different flow rates to analyze the influence of the liquid flow rate on the friction resistance. From Fig. 8(b), with the increasing of velocity, friction drag of both samples increased. According to Newton's law of viscosity, the force F are related to dynamic viscosity of fluid, the wetting area of test section and the velocity gradient, respectively. We can also see that the superhydrophobic surface has the low friction drag. The drag reduction ratio is about 33.3% compare with an untreated surface at a flow velocity of 0.8 m s^{-1}. When the flow velocity was about 4.5 m s^{-1}, the drag reduction ratio of the superhydrophobic surface reduced to 28.5%. The drag reduction radio is 20–30% for the as-prepared surface. Drag-reducing mechanism of the superhydrophobic surface is shown in Fig. 8(c). For the superhydrophobic surface, there is a bubble layer between the superhydrophobic solid surface and the nearest fluid layer. Under this condition, the nearest liquid–solid contacting mode was replaced with a liquid–gas–solid contacting mode. Correspondingly, the friction changed from the original solid–liquid friction (f) to the combination of solid–gas friction (f') and solid–liquid friction (f''). Considering that f' and f'' were both much lower than f, the friction force between the bubble and the fluid layer nearest the bubble layer, F' and F'', should also be much lower than F for the untreated surface. Since the Cassie fraction for a superhydrophobic surface can be very small, the liquid may efficiently flow over an air layer which allows the shear stress to be relieved over the gas layer near the solid. In simple terms, we can view this as a flow pattern evolving from a Poiseuille flow toward a plug flow. The liquid–gas interfaces replace the original liquid–solid interfaces partially, resulting in interfacial slippage, as shown in Fig. 6(c). The slippage induced by the entrapped gas is the main reason for the underwater drag reduction of the superhydrophobic surfaces.

4. Conclusions

We have proposed a novel method to fabricate superhydrophobic surface on a steel sheet using a high-temperature oxidation method in this paper. The oxidized steel surface has nanoflower structures. The as-prepared steel surface shows the superhydrophobic property. The water CAS is 158°, SA is less than 3°. The as-prepared surface has low adhesion ability. We have established an experimental setup to measure the liquid/solid friction. The drag reduction radio for the superhydrophobic surface is 20–30% at low velocity. We do believe that superhydrophobic surfaces may provide a promising application in the field of drag reduction for vehicle motions on or under the water surface.

References

1   G. X. Ke, G. Pan, Q. G. Huang, H. B. Hu and Z. Y. Liu, Review of underwater drag reduction technology, *Adv. Mech. Eng.*, 2009, **39**, 546–554.

2   D. Y. Zhang, Y. Y. Li, X. Han, X. Li and H. W. Chen, High precision bio-replication of synthetic drag reduction shark skin, *Chin. Sci. Bull.*, 2011, **56**, 938–944.

3   M. Zhou, J. Li, C. Feng, C. Wu, R. Yuan and L. Cai, Bionic Superhydrophobic and Drag-Reduction Properties on ZnO-Nanostructured Functional Surfaces, *Chem. Vap. Deposition*, 2011, **16**, 12–14.

4   M. Zhou, J. Li, C. X. Wu, X. K. Zhou and L. Cai, Fluid Drag Reduction on Superhydrophobic Surfaces Coated with Carbon Nanotube Forests (CNTs), *Soft Matter*, 2011, **7**, 4391–4396.

5   B. R. Solomon, K. S. Khalil and K. K. Varanasi, Drag Reduction using Lubricant-Impregnated Surfaces in Viscous Laminar Flow, *Langmuir*, 2014, **30**, 10970–10976.

6   Y. Wang, X. W. Liu, H. F. Zhang and Z. P. Zhou, Superhydrophobic surfaces created by a one-step solution-immersion process and their drag reduction effect on water, *RSC Adv.*, 2015, **5**, 18909–18914.

7   R. Fürstner and W. Barthlott, Wetting and Self-Cleaning Properties of Artificial Superhydrophobic Surfaces, *Langmuir*, 2005, **21**, 956–961.

8   Y. Y. Yan, N. Gao and W. Barthlottb, Mimicking natural superhydrophobic surfaces and grasping the wetting process: a review on recent progress in preparing superhydrophobic surfaces, *Adv. Colloid Interface Sci.*, 2011, **169**, 80–105.

9   K. Koch, B. Bhushan and W. Barthlott, Diversity of structure, morphology, and wetting of plant surfaces, *Soft Matter*, 2008, **4**, 1943–1963.

10 K. Koch, B. Bhushan and W. Barthlott, Multifunctional surface structures of plants: an inspiration for biomimetics, *Prog. Mater. Sci.*, 2009, **54**, 137–178.

11 X. F. Gao and L. Jiang, Biophysics: water-repellent legs of water striders, *Nature*, 2004, **432**, 36.

12 S. Wang and L. Jiang, Definition of superhydrophobic states, *Adv. Mater.*, 2007, **19**, 3423–3424.

13 X. J. Feng and L. Jiang, Design and creation of superwetting/antiwetting surfaces, *Adv. Mater.*, 2006, **18**, 3063–3078.

14 L. Wen, Y. Tian and L. Jiang, Bioinspired Super-Wettability from Fundamental Research to Practical Applications, *Angew. Chem., Int. Ed.*, 2015, **54**, 3387–3399.

15 Y. F. Gao, M. Nagai, Y. Masuda, F. Sato, W. S. Seo and K. Koumoto, Surface precipitation of highly porous hydrotalcite-like film on Al from a zinc aqueous solution, *Langmuir*, 2006, **22**, 3521–3527.

16 D. Kim, J. G. Kim and C. N. Chu, Aging effect on the wettability of stainless steel, *Mater. Lett.*, 2016, **170**, 18–20.

17 Y. Liu, Y. Bai, J. Jin, L. Tian, Z. Han and L. Ren, Facile fabrication of biomimetic superhydrophobic surface with anti-frosting on stainless steel substrate, *Appl. Surf. Sci.*, 2015, **355**, 1238–1244.

18 R. Jagdheesh, B. Pathiraj, E. Karatay, G. Römer and A. J. Huis in't Veld, Laser-Induced Nanoscale Superhydrophobic Structures on Metal Surfaces, *Langmuir*, 2011, **27**, 8464–8469.

19 J. Liang, D. Li, D. Wang, K. Liu and L. Chen, Preparation of stable superhydrophobic film on stainless steel substrate by a combined approach using electrodeposition and fluorinated modification, *Appl. Surf. Sci.*, 2014, **293**, 265–270.

20 T. Verho, C. Bower, P. Andrew, S. Franssila, O. Lkkala and R. H. Ras, Mechanically durable superhydrophobic surfaces, *Adv. Mater.*, 2011, **23**, 673–678.

21 X. Wen, S. Wang, Y. Ding, Z. L. Wang and S. Yang, Controlled growth of large-area, uniform, vertically aligned arrays of α-Fe_2O_3 nanobelts and nanowires, *J. Phys. Chem. B*, 2005, **109**, 215–220.

22 Y. Y. Fu, R. M. Wang, J. Xu, J. Chen, Y. Yan d, A. V. Narlikar and H. Zhang, Synthesis of large arrays of aligned α-Fe_2O_3 nanowires, *Chem. Phys. Lett.*, 2003, **379**, 373–379.

23 L. Gao and T. J. McCarthy, A perfectly hydrophobic surface, *J. Am. Chem. Soc.*, 2006, **128**, 9052–9053.

24 H. F. Zhang, L. Yin, L. Li, S. Y. Shi, Y. Wang and X. W. Liu, Wettability and drag reduction of a superhydrophobic aluminum surface, *RSC adv.*, 2016, **6**, 14034–14041.